Direct Hydrothermal Synthesis of $LiMn_2O_4$ Spinel and Lithium Ion Selective Adsorption

Qin-Hui Zhang, Shu-Ying Sun, Shao-Peng Li, Xian-Sheng Yin, Jian-Guo Yu

State Key Lab of Chemical Engineering, East China University of Science and Technology, Shanghai 200237, P. R. China, qhzhang@ecust.edu.cn

ABSTRACT

Spinel-type ternary $LiMn_2O_4$ oxides precursor was synthesized via directly hydrothermal synthesis of $Mn(NO_3)_2$, LiOH and H_2O_2 at 383 K for 8 h. The final low-dimensional MnO_2 nanorod ion-sieve with lithium ion selective adsorption property was prepared further by the acid treatment process to completely extract lithium ions from the Li-Mn-O lattice. The effects of hydrothermal reaction condition on the nanostructure, chemical stability and ion-exchange property of the $LiMn_2O_4$ precursor and MnO_2 ion-sieve were systematically examined via powder X-ray diffraction (XRD), high-resolution transmission electron microscopy (HRTEM), selected-area electron diffraction (SAED), N_2 adsorption-desorption and lithium ion selective adsorption measurements. The results show that this new kind of low-dimensional MnO_2 nanorod could be applied in lithium extraction from aqueous environment including brine, sea-water and waste water.

Keywords: $LiMn_2O_4$, hydrothermal synthesis, low-dimensional, ion-sieve, adsorption

1 INTRODUCTION

$LiMn_2O_4$ is a cubic spine1 with space group symmetry Fd3m. The Li^+ is transported via 8a-16d-8a channels in the three-dimensional interstitial space provided by the $[Mn_2O_4]$ framework in the $LiMn_2O_4$ spinel with little shrinking or swelling of the spinel structure [1]. The property makes the material applicable as cathode of lithium batteries [2, 3] and selective ion-sieves for lithium adsorption from aqueous solution including brine or seawater [4, 5].

Kenta Ooi and colleagues systematically researched the Li^+ selective adsorption on the λ-MnO_2 ion-sieve [6-8]. It should be noticed that the MnO_2 ion-sieve obtained by conversional solid-phase reaction is of irregular morphology and large aggregate with broad particle size distribution, though improved via the optimization of the synthesis conditions [9, 10]. Rationally, the soft chemistry hydrothermal-reaction is proposed to obtain $LiMn_2O_4$ spinel with homogeneous composition and nanosize distribution. Kenta Ooi and colleagues [11] make $LiMn_2O_4$ spinel via the hydrothermal-reaction of γ-MnO_2 or layered compound of Li-birnessite for about 24 days or longer, yet the raw material of γ-MnO_2 or Li-birnessite has to be firstly prepared via a complicated process [12-14]. In the present work, a much milder hydrothermal condition is optimized to synthesize low-dimensional spinel $LiMn_2O_4$ precursor directly. The final low-dimensional MnO_2 nanorod ion-sieve with lithium ion selective adsorption property was prepared further by the acid treatment process to completely extract lithium ions from the Li-Mn-O lattice; the structure characteristics and ion-exchange properties of the samples are studied by XRD, HRTEM, SAED, N_2 adsorption-desorption, and lithium ion selective adsorption measurement.

2 EXPERIMENTAL

2.1 Synthesis of Low-Dimensional $LiMn_2O_4$ Precursor and MnO_2 Ion-Sieve

All chemicals used are AR reagents. 300 ml mixed solution of H_2O_2 (0.20-0.90 $mol \cdot l^{-1}$) and LiOH (0.70-1.50 $mol \cdot l^{-1}$) is added dropwise into a teflon-coated stainless autoclave (1000 ml) filled with 300 ml 0.40 $mol \cdot l^{-1}$ $Mn(NO_3)_2$ solution stirred vigorously at 150 $r \cdot min^{-1}$. After the mixed solution maintained in air at room temperature for 2 h, the autoclave is sealed and heated at 343-453 K for 8-48 h respectively, then cooled naturally to room temperature. The obtained black precipitate is filtrated, washed completely with deionized water till the conductance of filtrate reaches the same level of the deionized water (about 18.2 $M\Omega \cdot cm^{-1}$) and dried at 343 K for 12 h. By optimizing the hydrothermal conditions of reaction temperature, contact time, concentration of H_2O_2 and LiOH solution, pure cubic $LiMn_2O_4$ ternary oxide, named LMO could be produced at 383 K for 8 h the mixed solution of 0.15 $mol \cdot l^{-1}$ H_2O_2, 0.50 $mol \cdot l^{-1}$ LiOH and 0.20 $mol \cdot l^{-1}$ $Mn(NO_3)_2$. The Li^+ extraction from $LiMn_2O_4$ precursor is carried out in 0.10 $mol \cdot l^{-1}$ HCl solution at 303 K until the lattice Li^+ is completely extracted (*in situ* measured by Metrohm 861 Advanced Compact Ion Chromatograph). The acid-treated materials are filtered, washed with deionized water and dried at 333 K for 8 h to obtain the final MnO_2 ion-sieve, named SMO. The whole process involves hydrothermal precipitation and redox procedure as the reaction (1) including three steps as equations (2)-(4). At high LiOH concentration (1.00 $mol \cdot l^{-1}$) the $Mn^{II}(OH)_2$ is oxidized accompanied with the Li^+ insertion into the Mn-O lattice to form the $LiMn^{III}Mn^{IV}O_4$ tri-oxide precursor.

Total reaction:

$Mn^{2+} + OH^- + Li^+ + H_2O_2 \rightarrow LiMn_2O_4 + H_2O$ (1)

Precipitation reaction:

$Mn^{2+} + 2\ OH^- \rightarrow Mn(OH)_2$ (2)

Redox reaction:

$Mn(OH)_2 + OH^- + H_2O_2 \rightarrow MnOOH + H_2O$ (3)

Li^+ insertion:

$Li^+ + MnOOH + H_2O_2 \rightarrow LiMn_2O_4 + H_2O$ (4)

2.2 Characterization of Samples

The bulky phase purity of the material is examined via X-ray diffraction (XRD) analysis using a Rigaku D/max 2550 X-ray diffractometer with Cu K_α radiation (λ=1.54056 Å), operating at 40 kV, 100 mA and scanning rate of $10°\cdot min^{-1}$. The microstructure and surface morphology of the samples are analyzed by HRTEM and SAED on a JEOL JEM-2100F TEM (200 kV) after the samples are dispersed by ultrasonic in anhydrous ethanol for 5 min and then placed onto the cuprum grid for observations. The texture detail is characterized by N_2 adsorption-desorption at 77 K using Micromeritics ASAP 2010 V5.02, and the surface area is calculated from the Brunauer-Emmett-Teller (BET) equation, and pore volume from the total amount of nitrogen adsorbed at relative pressures of ca. 0.96 with Barrett-Joyner-Halenda (BJH) equation.

2.3 Lithium Ion Adsorption Measurement

The Li^+ adsorption isotherm is carried out by stirring ($150\ r\cdot min^{-1}$) about 100 mg ion-sieve in 100 ml LiCl solution (pH = 10.1 adjusted by buffer solution comprised of 0.1 $mol\cdot l^{-1}$ NH_4Cl and 0.1 $mol\cdot l^{-1}$ $NH_3\cdot H_2O$, the molar ratio equal to 0.25) with different initial Li^+ concentration for about 72 h at 303 K. The final adsorption isotherm is simulated according to Freundlich equation of $Q_e = k\cdot C_e^{1/n}$. The Li^+ adsorption kinetics is carried out by stirring ($150\ r\cdot min^{-1}$) about 100 mg ion-sieve in 100 ml LiCl solution (pH = 10.1) with uniform initial Li^+ concentration (10.0 $mmol\cdot l^{-1}$) at 303 K. The final adsorption kinetics is simulated according to the first order rate Lagergren equation of $\ln (Q_e-Q_t) = \ln Q_e - k_{ads}\cdot t$. The selectivity of Li^+ compared with other coexisting cations is carried out by stirring about 100 mg ion-sieve in 10 ml mixed solution (pH = 10.1) containing Li^+, Na^+, K^+, Ca^{2+} and Mg^{2+} of 10.0 $mmol\cdot l^{-1}$ respectively for 72 h at 303 K. The concentration of all metal ions in supernatant lucid solution is determined *in situ* by IC until the attainment of equilibrium. The exchange capacity or the amount of metal ion adsorbed per gram of ion-sieve at equilibrium (Q_e), distribution coefficient (K_d), separation factor (α^{Li}_{Me}) and concentration factor (CF) are calculated according to equations (5)-(8).

$Q_e = (C_0-C_e)\cdot V / W$ (5)

$K_d = (C_0-C_e)\cdot V / (C_e\cdot W)$ (6)

$\alpha^{Li}_{Me} = K_d\,(Li) / K_d\,(Me)$ Me: Li, Na, K, Ca and Mg (7)

$CF = Q_e\,(Me) / C_0\,(Me)$ (8)

3 RESULTS AND DISCUSSION

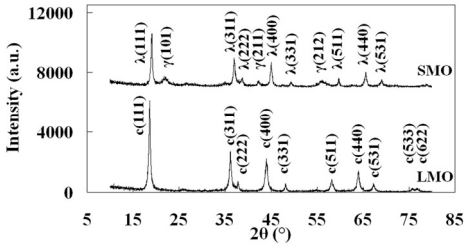

Figure 1: XRD patterns of LMO precursor and SMO ion-sieve. c(hkl): cubic $LiMn_2O_4$ crystal face; λ(hkl): cubic MnO_2 crystal face; r(hkl): ramsdellite MnO_2.

The powder X-ray diffraction patterns of the nanocrystal $LiMn_2O_4$ precursor (LMO) and MnO_2 ion-sieve (SMO) are presented in Figure 1. The reflections of LMO can be readily indexed to pure cubic phase [S.G.: Fd3m(227)] of $LiMn_2O_4$ with lattice constant of a = 8.248 Å (JCPDS 35-0782), and the reflections of SMO, to cubic phase [S.G.: Fd3m(227)] of λ-MnO_2 with lattice constant a = 8.030 Å (JCPDS 44-0992). The several faint diffraction peaks at 22.16°, 42.44° and 56.24° indicate trace amounts of orthorhombic phase [S.G.: Pnma(62)] of ramsdellite-MnO_2 (JCPDS 39-0375, a = 9.270 Å, b = 2.866 Å, c = 4.533 Å). The phenomena are different from those of spinel $LiMn_2O_4$ prepared by calcination method in related work, in which the $LiMn_2O_4$ precursor and the final MnO_2 ion-sieve fully present the same spinel-type structure and the relative peak intensities corresponding to (111) and (400) planes are also weaker [10]. These are probably resulted from the relatively low stability of $LiMn_2O_4$ without high temperature crystallization process and further research to obtain pure cubic phase MnO_2 ion-sieve is still in process. However, it should be noticed that the XRD patterns of LMO and SMO are still quite similar, indicating that the Mn-O lattice is stable during the Li^+ extraction process and the locations of manganese in the crystal structure are well maintained as the $LiMn_2O_4$ counterpart of solid-phase reaction.

The present synthesis conditions have been greatly alleviated and the morphology of the $LiMn_2O_4$ precursor and final MnO_2 ion-sieve is effectively controlled within low-dimensional nanorod structure as shown in Figure 2. The $LiMn_2O_4$ precursor yields mainly mono-dispersed nanorods with about 20 nm in diameter and several micrometers in length as shown in Figure 2 LMO (A), implying that the soft chemistry synthesis is effect for the direct formation of low-dimensional $LiMn_2O_4$ ternary nanostructure with quite uniform geometry, evidenced further by the pore size distribution curve obtained from the BJH deposition curve (as shown in Figure 3) with a pore size distribution centered on 30.9 nm. The pore size distribution, unlike the HRTEM observations, is obtained statistically, thus the appearance of the obviously broad peak is attributed to capillary condensation in the slit-

Clean Technology 2008, www.ct-si.org, ISBN 978-1-4200-8502-0

shaped meso-pores with parallel walls and implies the separation of most nanorods from one another although some of the nanorods look thicker than others. Figure 2 LMO (B) is a typical HRTEM image of a single $LiMn_2O_4$ nanorod with inset of SAED pattern recorded on the selected area, showing reflection characteristic of one-dimensional nanorod structure, with the diffraction spots elongated in the direction perpendicular to the rod axis, and the SAED pattern also confirms that the $LiMn_2O_4$ ternary oxide is single crystal. The SMO ion-sieve affords the similar one-dimensional nanorod morphology with $LiMn_2O_4$ precursor as shown in Figure 2 SMO (A), without aggregation after the acid treatment process evidenced further by the pore size distribution curve (as shown in Figure 3) with a pore size distribution centered on 31.9 nm. Figure 2 SMO (B) is a typical HRTEM image of a single MnO_2 nanorod with the diameter of about 20 nm and the corresponding SAED pattern (inset) indicating that the nanorod is single crystal with the growth direction along the (111) lattice face (as shown in the arrow direction).

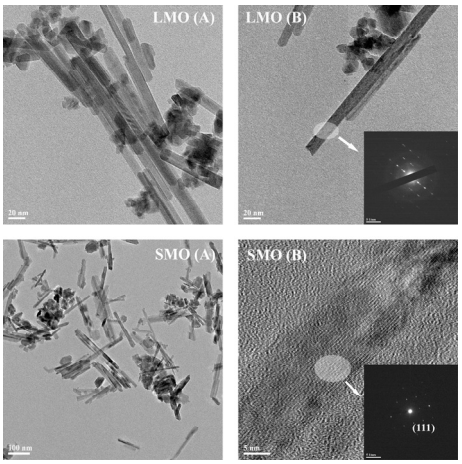

Figure 2: HRTEM images of LMO precursor and the SMO ion-sieve with the insets of SAED patterns respectively.

Figure 3 shows the N_2 adsorption-desorption isotherm of LMO precursor and SMO ion-sieve. The N_2 adsorption capacity of SMO ion-sieve (310 $cm^3 \cdot g^{-1}$, STP) is much larger than that of LMO precursor (170 $cm^3 \cdot g^{-1}$, STP), indicating that more meso-pores are developed after Li^+ extracted from the precursor. In both cases, the isotherm contains H3-type hysteresis loop with a delayed desorption branch generally occurred for capillary adsorption into interstices of compact meso-pores. The physical chemistry texture property of LMO precursor and the SMO ion-sieve are shown in Table 1. The specific surface areas (S_{BET}) accordingly increased from 57.85 $m^2 \cdot g^{-1}$ of the $LiMn_2O_4$ precursor to 75.75 $m^2 \cdot g^{-1}$ of the final MnO_2 ion-sieve after Li^+ are extracted from the Li-Mn-O lattice, contrast to the phenomena of solid-phase reaction process, in which high temperature calcinations resulted in serious aggregation of the $LiMn_2O_4$ and MnO_2 bulky particles. Pore size distribution analysis via the DFT method, applicable for a complete range of pore size indicates that both the samples afforded a mesoporeous size distribution with the peak pore size (D_p) centered on 30.9 nm of LMO and 31.9 nm of SMO respectively. In both cases, the values of external surface area (S_e) and S_{BET} are similar, reflecting again the lack of micropores in these samples and the very little micropore volume is also observed.

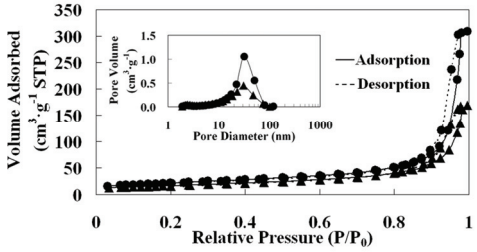

Figure 3: N_2 adsorption-desorption isotherm and pore size distribution curve (inset) of LMO and SMO. ●: LMO, ▲: SMO.

	S_{BET} $m^2 \cdot g^{-1}$	S_e $m^2 \cdot g^{-1}$	V_T $cm^3 \cdot g^{-1}$	Hysteresis Loop	D_p nm
LMO	57.85	55.56	0.18	H3	30.9
SMO	75.75	72.94	0.34	H3	31.9

Table 1: Physical chemistry texture of LMO precursor and SMO ion-sieve

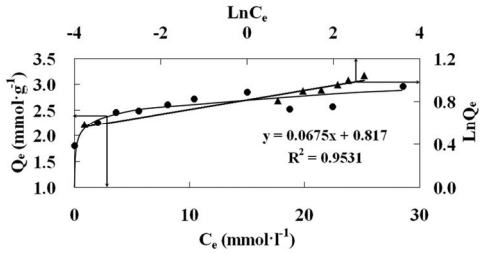

Figure 4: Li^+ adsorption isotherm of SMO nanorod ion-sieve and simulation according to Freundlich equation. T = 303 K, pH = 10.1, V = 100 ml, W = 100 mg.

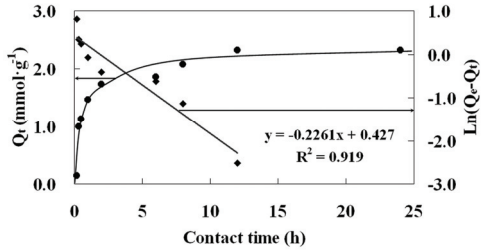

Figure 5: Li^+ adsorption kinetics of SMO nanorod ion-sieve and simulation according to Lagergren equation. T =303 K, pH = 10.1, V= 100 ml, W = 100 mg, C_0 = 10 $mmol \cdot l^{-1}$.

Figure 4 shows the Li^+ adsorption isotherm of the SMO nanorod ion-sieve and simulation according to Freundlich equation. The data present linearity with the congruence of R^2 = 0.9531, indicating that the Li^+ adsorption process in the experiment is accorded with the Freundlich adsorption isotherm. The adsorption constants are calculated to be K_f = 2.26 and n = 14.81. Although the value is only a little higher than that of the bulky MnO_2 ion-sieve (2.43 mmol·g^{-1}) synthesized by high-temperature calcination method [10], it is probable that the current nanorod MnO_2 contains trace amounts of ramsdellite-MnO_2 besides the cubic phase MnO_2 (as shown in Fig. 1) and the ramsdellite-MnO_2 has great defect to the Li^+ insertion process. Further research on the pure cubic phase nanorod MnO_2 synthesis is undergoing. Figure 5 shows the Li^+ adsorption kinetics of SMO nanorod ion-sieve and simulation according to Lagergren equation. The adsorption rate is fast till the contact time of 2 h, then the adsorption rate increases slowly and the process is close to the equilibrium. The value of the adsorption rate constant is calculated to be $K_{ads} = 6.28\times10^{-5}$ s^{-1}. The adsorption rate improves one order compared with bulky MnO_2 ion-sieve ($K_{ads} = 2.17\times10^{-6}$ s^{-1}) [10], indicating that the morphology and size of the ion-sieve have apparent influence on the Li^+ adsorption rate.

Metal Ion	Q_e mmol·g^{-1}	K_d ml·g^{-1}	α^{Li}_{Me}	CF $\times10^{-3}$ l·g^{-1}
Li^+	0.967	16770.63	1.00	95.42
Na^+	0.009	1.07	15640.12	1.06
K^+	0.004	0.46	36066.14	0.46
Mg^{2+}	0.126	15.47	1084.27	13.32
Ca^{2+}	0.230	32.26	519.80	24.15

Table 2: Adsorption selectivity of Li^+ on SMO ion-sieve.

Table 2 shows the selectivity of Li^+ compared with uptake behaviors of other coexisting ions in brine including Na^+, K^+, Ca^{2+} and Mg^{2+}. The equilibrium distribution coefficients K_d are in the order of $Li^+ >> Ca^{2+} > Mg^{2+} > Na^+ > K^+$, indicating high selectivity for Li^+, but much less for Na^+, K^+, Ca^{2+}, and Mg^{2+}, similar to the cases of the MnO_2 ion-sieves prepared by solid-phase reaction, yet there exist more obvious discriminations among the values of K_d and α^{Li}_{Me}. The distribution coefficients for Li^+ is $K_{d,\ Li}$ = 16770.63 ml·g^{-1}, increased about 2.12 times compared with the bulky MnO_2 ion-sieve ($K_{d,\ Li}$ =7917.49 ml·g^{-1}) [10], indicating the remarkable improvement of the ion-sieve selectivity by the well-maintained nanorod structure. The results also indicate that Na^+, K^+, Ca^{2+} and Mg^{2+} in solution do not interfere with Li^+ during the adsorption/ion-exchange process since high concentration factor (CF) values of Li^+ are observed as compared with CF values of other metal ions [11].

4 CONCLUSION

One-dimensional spinel-type $LiMn_2O_4$ nanorod oxide, with the average size about 20 nm in diameter and several micrometers in length, has been directly synthesized via a simple hydrothermal synthesis of commercial $Mn(NO_3)_2$, LiOH and H_2O_2 mixed solution at 383 K for 8 h, more favourable to control the nanocrystalline structure with well-defined pore size distribution and high surface area than traditional calcinations method, which is of great interest as an electrode material for rechargeable lithium-ion batteries. Further, the final MnO_2 ion-sieve with lithium ion selective adsorption capacity could be easily prepared via the acid treatment process to completely extract lithium ions from the spinel Li-Mn-O precureor, without obvious change to the Mn-O lattice structure and the one-dimensional nanorod morphology; the Li^+ selective adsorption behaviors of the MnO_2 nanorod ion-sieve are improved compared with those prepared by the conventional calcinations method, which is promising in the lithium extraction from brine or seawater.

ACKNOWLEDGMENTS

This work was supported by NSFC (No. 20576031 and 20706014), Rising-star Project of STCSM (No. 05QMX1414) and National 863 Project (No. 2008AA06Z111).

REFERENCES

[1] A. Van der Ven, C. Marianetti, Morgan D, et al., Solid State Ionics, 135, 21, 2000.
[2] M. Nishizawa, T. Ise, H. Koshika, et al., Chem. Mater., 12: 1367, 2000.
[3] B. Ammundsen, J. Paulsen, Adv. Mater., 13, 943, 2001.
[4] K. Ooi, Y. Miyai, J. Sakakihara, Langmuir, 7, 1167, 1991.
[5] Q. Feng, H. Kanoh, K. Ooi, J. Mater. Chem., 9, 319, 1999.
[6] K. Ooi, Y. Miyai, S. Katoh, Sep. Sci. Technol., 21, 755, 1986.
[7] K. Ooi, Y. Miyai, S. Katoh, et al., Langmuir, 5, 150, 1989.
[8] Q. Feng, Y. Miyai, H. Kanoh, et al., Langmuir, 8, 1861, 1992.
[9] Q. H. Zhang, S. Y. Sun, S. P. Li, et al., Int. J. Chem. React. Eng., 5, 1, 2007.
[10] Q. H. Zhang, S. Y. Sun, S. P. Li, et al., Chem. Eng. Sci., 62, 4869, 2007.
[11] Q. Feng, K. Ooi, H. Kanoh, et al., Chem. Mater., 7, 1226, 1995.
[12] Q. Feng, Y. Higashimoto, K. Kajiyoshi, et al., J. Mater. Sci. Lett., 20, 269, 2001.
[13] T. Kanasaku, K. Amezawa, N. Yamamoto, Solid State Ionics, 133, 51, 2000.
[14] Y. C. Zhang, H. Wang, H. Y. Xu, et al., Solid State Ionics, 158, 113, 2003.